JACS
JOURNAL OF THE AMERICAN CHEMICAL SOCIETY
Article
pubs.acs.org/JACS

De Novo-Designed Metallopeptides with Type 2 Copper Centers: Modulation of Reduction Potentials and Nitrite Reductase Activities

Fangting Yu, James E. Penner-Hahn, and Vincent L. Pecoraro*

Department of Chemistry, University of Michigan, 930 North University Avenue, Ann Arbor, Michigan 48109-1055, United States

Supporting Information

ABSTRACT: Enzymatic reactions involving redox processes are highly sensitive to the local electrostatic environment. Despite considerable effort, the complex interactions among different influential factors in native proteins impede progress toward complete understanding of the structure−function relationship. Of particular interest is the type 2 copper center $Cu(His)_3$, which may act as an electron transfer center in peptidylglycine α-hydroxylating monooxygenase (PHM) or a catalytic center in copper nitrite reductase (CuNiR). A de novo design strategy is used to probe the effect of modifying charged amino acid residues around, but not directly bound to, a $Cu(His)_3$ center embedded in three-stranded coiled coils (**TRI-H**)$_3$ [**TRI-H** = Ac-G WKALEEK LKALEEK LKALEEK **H**KALEEK G-NH_2]. Specifically, the peptide **TRI-EH** (=**TRI-H**K22E) alters an important lysine to glutamate just above the copper binding center. With a series of **TRI-EH** peptides mutated below the metal center, we use a variety of spectroscopies (EPR, UV−vis, XAS) to show a direct impact on the protonation equilibria, copper binding affinities, reduction potentials, and nitrite reductase activities of these copper−peptide complexes. The potentials at a specific pH vary by 100 mV, and the nitrite reductase activities range over a factor of 4 in rates. We also observe that the affinities, potentials, and catalytic activities are strongly influenced by the pH conditions (pH 5.8−7.4). In general, Cu(II) affinities for the peptides are diminished at low pH values. The interplay among these factors can lead to a 200 mV shift in reduction potential across these peptides, which is determined by the pH-dependent affinities of copper in both oxidation states. This study illustrates the strength of de novo protein design in elucidating the influence of ionizable residues on a particular redox system, an important step toward understanding the factors that govern the properties of this metalloenzyme with a goal of eventually improving the catalytic activity.

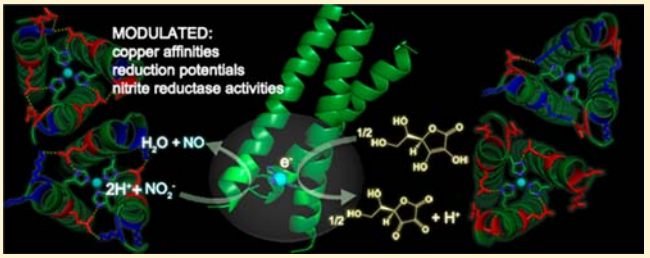

INTRODUCTION

Redox-active enzymes are critical in many biological processes, with metal cofactors accounting for many of the redox-related reactions in native proteins. These activities include catalyzing important biological processes such as photosynthesis (electron transfer and water oxidation), respiration, molecular oxygen reduction, nitrogen fixation, and denitrification.[1−5] Specifically, redox-active copper sites exist in a large number of metalloproteins, which, along with iron proteins, play important roles in electron transfer, activation and transport of dioxygen, and the metabolism of other small molecules.[6−16] Within the metallobiosphere, copper proteins are extremely important, with functions ranging from pure electron transfer to multielectron redox catalysis. Type 2 copper centers comprise a broad class of mononuclear sites that again serve both catalytic and redox functions. Two specific enzymes are of interest to us as they contain $Cu(His)_3$ structures. The first, peptidylglycine α-hydroxylating monooxygenase (PHM), has a $Cu(His)_3$ center (Cu_H) whose role is to donate an electron to the catalytic Cu_M site that activates dioxygen.[17−20] The second, copper nitrite reductase (NiR), is an essential component of dissimilatory nitrite reduction using a type 1 Cu center to donate an electron to the $Cu(His)_3$ active site, which along with protons converts NO_2^- to NO and H_2O.[7,21−25] Thus, a structurally related $Cu(His)_3$ site can be differentially utilized on the basis of the surrounding protein environment.

Understanding the relationship between structure and function has always been a major goal of biomimetic studies. For redox-active metalloproteins, it is obvious that the ligands coordinated to the metal center directly influence the redox properties.[26,27] However, electrostatic interactions of the redox center with the surrounding charged groups are now recognized to influence redox property modulation. Charged amino acid residues [e.g., glutamate (Glu) and lysine (Lys)] both in the interior and on the surface of the proteins can participate in fine-tuning the potentials of redox-active metal sites.[28−31] Furthermore, enzymatic reactions can be highly sensitive to the local electrostatic environment. Considerable effort has been devoted to understanding the electrostatic interactions in native proteins, but because of the complexity of native systems, it is always challenging to disentangle the contributions of the potentially influential factors.

Received: June 30, 2013
Published: November 1, 2013

dx.doi.org/10.1021/ja406648n | J. Am. Chem. Soc. 2013, 135, 18096−18107

Table 1. Peptide Sequences Used in This Study[a]

Peptide[b]	Sequence	Δ_{charge}[c]
	a b c d e f g a b c d e f g a b c d e f g a b c d e f g	
TRI-H	Ac-G WKALEEK LKALEEK LKALEEK **H**KALEEK G-NH_2	---
TRI-HK22Q	Ac-G WKALEEK LKALEEK LKALEE**Q** **H**KALEEK G-NH_2	-3
TRI-EHE27K	Ac-G WKALEEK LKALEEK LKALEE**E** **H**KAL**K**EK G-NH_2	0
TRI-EHE27Q	Ac-G WKALEEK LKALEEK LKALEE**E** **H**KAL**Q**EK G-NH_2	-3
TRI-EH	Ac-G WKALEEK LKALEEK LKALEE**E** **H**KALEEK G-NH_2	-6
TRI-EHK24Q	Ac-G WKALEEK LKALEEK LKALEE**E** **H**Q**A**LEEK G-NH_2	-9
TRI-EHK24E	Ac-G WKALEEK LKALEEK LKALEE**E** **H**E**A**LEEK G-NH_2	-12

[a]The color code used throughout corresponds to a change of charge compared to a single **TRI-H** peptide. A difference of −2 charges is given in red, −1 in magenta, +1 in purple, and +2 in blue. [b]The C-terminus is capped by an NH_2 group and the N-terminus by an acetyl (Ac) group. [c]Δ_{charge} is defined as the difference in total charge of the specified 3SCC versus $(\mathbf{TRI\text{-}H})_3$ assuming all Glu are fully deprotonated and all Lys are fully protonated. Polyglutamate or polylysine based ligands can exhibit a wide range of pK_a values when multiple side chains of the same type occur in the same peptide. Therefore, one should recognize that nonintegrally charged peptides can exist due to incomplete acid−base chemistry.

A de novo design strategy provides an opportunity to generate biologically relevant models to understand structure−function relationships using a minimal construct.[32−35] With a simplified polypeptide sequence, the local environment of metal centers may be modified rationally in order to investigate the important factors that govern the properties and functions of a specific site. Previously, we reported a functional copper nitrite reductase model embedded in a de novo-designed three-stranded coiled coil (3SCC) scaffold, which represents one of the most efficient model systems for NiR in aqueous solutions.[36] Prior to that work, there were a few cases of $Cu(His)_3$ sites in de novo-designed peptides with controlled copper coordination.[37−39] Although redox processes have been demonstrated in a few systems,[40,41] none were fully characterized in both oxidation states. Our system was the first to have both relatively well-characterized, stable Cu(I) and Cu(II) oxidation states that exhibits NiR activity under aqueous conditions. We observed very positive reduction potentials for these systems, which probably reflected the stabilization of the Cu(I) state in a trigonal-planar geometry.[36] Initial designs focused solely on the first coordination sphere of copper, yielding modest catalysts. To design a model with higher rates, the next logical step is to explore systematically secondary coordination sphere modifications around the copper. Of course, such studies are potentially relevant to understanding how solely electron transfer centers as found in PHM are influenced by the same secondary coordination sphere modifications. We report herein a series of modified peptides (Table 1) based on the parent peptide **TRI**L2WL23H (**TRI-H**) that address how the local environment, particularly charged residues, influence the redox properties and catalytic behaviors of these designed copper proteins. Models of Cu(I)$(\mathbf{TRI\text{-}H})_3$ and the other peptides used are given in Figure 1.

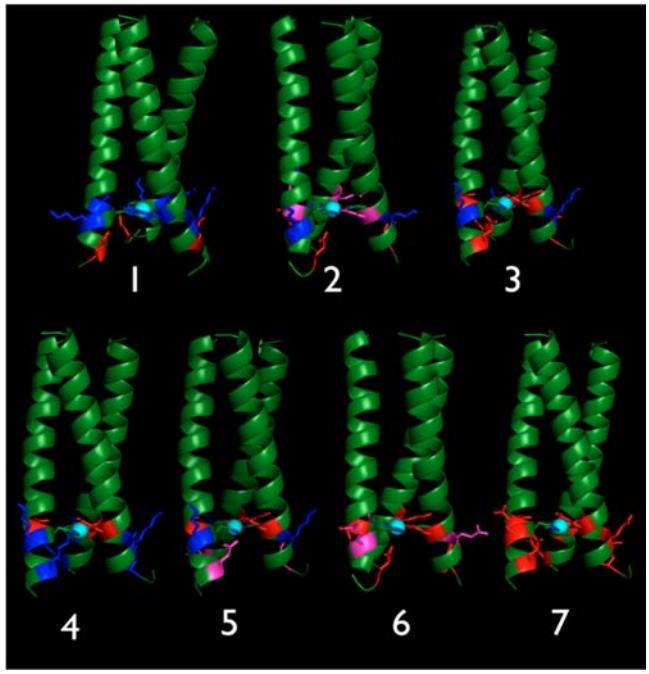

Figure 1. PyMOL models of (1) **TRI-H**, (2) **TRI-H**K22Q, (3) **TRI-EH**, (4) **TRI-EH**E27K, (5) **TRI-EH**E27Q, (6) **TRI-EH**K24Q, and (7) **TRI-EH**K24E from the left to the right based on the crystal structure of $Zn(II)_{-N}Hg(II)_{-S}(\mathbf{CS}L9PenL23H)_3$ (PDB code 3pbj).[42]

EXPERIMENTAL METHODS

The sequences of the peptides used in this work are shown in Table 1, with each heptad repeat given as *abcdefg*. Variations were made at the *b*, *e*, and *g* positions of the heptad in addition to the L23H mutation.

General Procedures. The copper−peptide complexes were prepared by adding a solution of tetra(acetonitrile)copper(I) tetrafluoroborate or copper(II) chloride into a (buffered) solution of apo-peptide. Since the Cu(I)−peptide complexes undergo slow oxidation under aerobic conditions, all of the reactions involving Cu(I) or nitrite reduction were carried out in an inert atmosphere box.

Peptide Synthesis and Purification. All of the peptides in this work were synthesized on an Applied Biosystems 433A peptide synthesizer using standard protocols[43] and purified and characterized as previously reported.[44] The apo-peptide solution was prepared by dissolving purified dry peptides in doubly distilled water or buffer solutions. The peptide concentration was determined on the basis of the tryptophan (Trp) absorbance at 280 nm (ε = 5500 M^{-1} cm^{-1}).[45]

UV−Vis and Fluorescence Spectroscopy. UV−vis spectra were collected in airtight quartz cuvettes at 25 °C on a Cary 100 Bio UV−vis spectrophotometer. Emission spectra were recorded on a FluoroMax-2 fluorimeter at 25 °C.

pK_a Determination for Cu(II)−Peptide Complexes. The deprotonation of Cu(II)−peptide complexes was reflected in the UV−vis spectra. The UV−vis spectra of a solution containing 0.27 mM Cu−3SCC and 0.03 mM apo-3SCC [to ensure that >99% of the Cu(II) was bound to the peptide] under various pH conditions were collected and pK_a was fitted to eq 1. The protonation equilibrium corresponding to *n* protons can be described as follows:

$$EH_n \overset{K_a^n}{\rightleftarrows} nH^+ + E^{n-}$$

The total molar extinction coefficient at a particular wavelength can be written as

$$\varepsilon_{total} = \frac{\varepsilon_E + \varepsilon_{EH_n} \cdot 10^{n(pK_a - pH)}}{1 + 10^{n(pK_a - pH)}} \quad (1)$$

where ε_E and ε_{EH_n} stand for the extinction coefficients of individual species in different protonation states.

Determination of Binding Constants. *Cu(I) Binding Constants.* The affinities of peptide trimers (pep_3) to Cu(I) were determined by competitive binding assays with disodium bathocuproindisulfonate (Na_2BCS, BCS) or disodium bacinchoninate (Na_2BCA, BCA) as a competitive chelator in 50 mM potassium phosphate buffer. The competition equilibrium for the titration experiment can be expressed by the following chemical equation:

$$Cu{-}pep_3 + 2L \rightleftarrows CuL_2 + pep_3$$

where L = BCS or BCA. Starting with 40 μM Cu(I)−pep_3 and 40 μM apo-pep_3, small aliquots of a 5.00 mM BCS or BCA stock solution were added into the system. Transfer of Cu(I) from Cu−pep_3 to CuL_2 was tracked from the absorbance at 483 nm for L = BCS (ε = 13 000 M^{-1} cm^{-1}) or 562 nm for L = BCA (ε = 7900 M^{-1} cm^{-1}).[46−48] Titrations were carried out in triplicate, and the dissociation constants were fitted using the spectrophotometric and/or potentiometric data fitting program Hyperquad 2006 and the reported dissociation constants for $Cu(I)L_2$.[46−48] Titrations were performed at both pH 7.4 and pH 5.8 to investigate how the affinities change in relation to pH. At pH 5.8, the concentration of the protonated form of the ligand BCS was taken into account.[47,48]

Cu(II) Binding Constants. As reported previously, the Trp emission at 350 nm decreases upon Cu(II) binding to the $(His)_3$ pocket.[36] A stock solution of $CuCl_2$ was added to ∼800 nM 3SCC in 50 mM buffer solution. Triplicate titrations were carried out, and the data were fitted with Hyperquad 2006.

X-ray Absorption Spectroscopy (XAS). A 1 mM Cu(I)(**TRI-EH**)$_3$ solution was prepared by adding 0.8 equiv (with respect to peptide trimer) of tetra(acetonitrile)copper(I) tetrafluoroborate solution to the peptide buffer solution in an inert atmosphere box. The pH of the solution was adjusted to 8.5 using small aliquots of concentrated KOH. Glycerol was added as a glassing agent. The homogeneous 50% aqueous glycerol solution was then transferred to a sample cell and frozen at liquid nitrogen temperature. Data were collected at the Stanford Synchrotron Radiation Lightsource (SSRL) on beamline 7-3 with a Si(220) double-crystal monochromator, a flat Rh-coated harmonic rejection mirror, and a 30-element Ge array detector. An Oxford Instruments liquid helium cryostat was used to keep the samples below 10 K during data collection. Data were collected as fluorescence excitation spectra and normalized to the incident intensity measured with a N_2-filled ion chamber. Data were measured with steps of 0.25 eV in the X-ray absorption near-edge structure (XANES) region (1 s integration time) and k = 0.05 to 13.5 $Å^{-1}$ in the extended X-ray absorption fine structure (EXAFS) region (1−20 s integration, k^3-weighted). Energies were calibrated by assigning the lowest-energy inflection point of a copper metal foil as 8980.3 eV. An initial E_0 value of 9000 eV was used to convert data to k space, and the background was removed using a three-region cubic spline. The EXAFS data were analyzed using EXAFSPAK[49] with ab initio amplitude and phase parameters calculated using FEFF 9.0.[50] Imidazole outer-shell scattering was modeled using phase and amplitude parameters calculated for an idealized $Cu(imid)_4$ structure with Debye−Waller factors defined as suggested by Dimakis and Bunker;[51] the imidazole was refined as a rigid group with distances and Debye−Waller factors linked to the refined Cu−N parameters, so there were only three variable parameters (R_{Cu-N}, σ^2_{Cu-N}, and ΔE_0).

Electron Paramagnetic Resonance (EPR) Spectroscopy. X-band EPR spectra were collected on a Bruker EMX electron spin resonance spectrometer with a Varian liquid nitrogen cryostat at 77 K. A sample of ∼1 mM Cu(II)$(3SCC)_3$ was prepared in a 50 mM buffer solution, and the pH was adjusted by adding concentrated HCl or KOH solution to the sample. An extra 0.5 mM apo-3SCC was added to ensure that the free Cu(II) was less than 0.1%, and 50% glycerol was used as a glassing agent. The EPR parameters were extracted by fitting the collected spectra to the simulated spectra using the EPR data fitting software SpinCount.

NiR Activity Reaction Rates. The rates were determined as previously reported for Cu(**TRI-H**)$_3$.[36] $NaNO_2$ (30 mM) was mixed with 0.18 mM Cu(II)(3SCC) and 0.09 mM apo-3SCC [to ensure that over 99% of the Cu(II) was bound to the peptide]. The reaction was initiated by adding 6 equiv of sodium ascorbate (NaAsc) with respect to Cu(II). The consumption of NaAsc was monitored by UV−vis spectroscopy. The control was a mixture of 30 mM $NaNO_2$ and 0.09 mM apo-3SCC with the same amount of NaAsc. The rates of the reaction were calculated as 2 times the difference in rates of NaAsc consumption (decrease of absorbance at 251 nm) for the sample and the control. The production of nitric oxide was examined using the method previously reported.[36]

RESULTS

pK_a of Cu(II)−Peptide Complexes. For the parent peptide **TRI-H**, the appearance of a broad band with a maximum absorbance at 644 nm was observed as the pH of a Cu(II)(**TRI-H**)$_3$ solution was increased from 2.92 to 5.52 (Figure 2A). This spectrum has previously been suggested to be due to $Cu(II)(His)_3(OH_2)_{1-2}$.[36] When the pH was raised above 7.6, a new set of spectra containing an isosbestic point at 571 nm was observed (Figure 2B). The absorbance at 644 nm decreased while a new band at 514 nm grew in intensity. From a fit of the absorbance at 644 nm to eq 1, a pK_a^w value corresponding to the changes in the absorption spectra

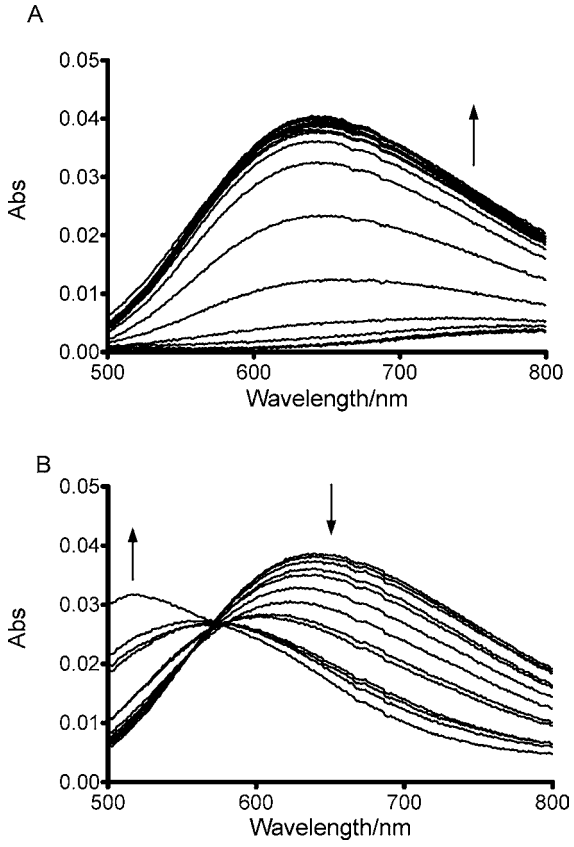

Figure 2. pH titration spectra of Cu(II)(**TRI-H**)$_3$ at (A) lower pH (2.92−7.45) and (B) higher pH (7.60−10.80).

dx.doi.org/10.1021/ja406648n | J. Am. Chem. Soc. 2013, 135, 18096−18107

described above was extracted (Table 2); this value corresponds to a one-proton deprotonation process.

Table 2. pK_a Values[a] and Spectroscopic Parameters of Selected Cu(II)−Peptides

			λ_{max}/nm (ε/M^{-1} cm^{-1})	
peptide	pK_a^E	pK_a^w	pH 5.8	pH 7.4
TRI-H		8.53(2)	644 (143)	644 (143)
TRI-EHE27K		9.59(15)	671 (80)	671 (79)
TRI-EH	6.33(4)	9.86(5)	659 (110)	659 (89)
TRI-EHK24E	6.76(6)	9.81(5)	665 (101)	657 (81)

[a]The two pK_a values correspond to two different deprotonation processes. pK_a^E is associated with Glu22 and pK_a^w is associated with the Cu(II)-bound water.

Interestingly, the pH titration of Cu(II)(**TRI-EH**)$_3$ resulted in pK_a values distinctively different from that of the parent peptide (Table 2). Again, in the pH region 2.97−5.57, the increase in the absorbance at 659 nm is indicative of binding of copper to the peptide and is reminiscent of the parent peptide (Figure S1 in the Supporting Information). However, when the pH was raised from 5.33 to 7.87, the absorbance at 659 nm decreased slightly (Figure 3), resulting in a pK_a^E value of 6.33.

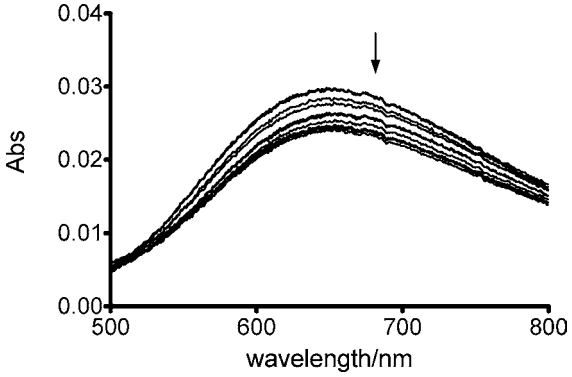

Figure 3. pH titration spectra of Cu(II)(**TRI-EH**)$_3$ between pH 5.33 and pH 7.87.

This deprotonation event fitted best to a 1.65(23) proton process (Figure S1B), which suggested that the nature of this deprotonation might be different from the one for Cu(II)(**TRI-H**)$_3$. Similar effects were also observed for Cu(II)(**TRI-EH**K24E)$_3$ (Figure S2). The Cu(II) d−d band evolved differently upon pH increase for different peptides within the pH region of interest to us (Figure 4). In summary, we observed the appearance of a Cu(II) d−d band when Cu(II) was bound to different peptides, and the transformations of the spectra were pH-dependent because of various deprotonation events.

Cu(I) and Cu(II) Affinities, Free Energies of Binding, and Calculated Reduction Potentials. Dissociation constants for the complexation of either Cu(I) or Cu(II) at pH 5.8 and 7.4 for each of the peptides studied in this work are provided in Table 3. The first point to recognize is that the reversal of the position of the Lys and Glu groups in going from **TRI-H** to **TRI-EH**E27K leads to a marked change in the Cu(I) affinity (a factor of 100 in favor of the reversed peptide), while the corresponding Cu(II) affinities are higher for the original parent peptide. In an effort to isolate the effects, peptides solely with modifications at position 22, which is much closer to the copper site than position 27 (Figure 1), were examined. At pH 7.4, for the series **TRI-EH**, **TRI-H**K22Q, and **TRI-H**, corresponding to Δ_{charge} = −6, −3, and 0, respectively, the Cu(I) affinity changed only modestly (a factor of 5 less stable for **TRI-H**K22Q and essentially identical for **TRI-EH**) and the Cu(II) affinities were essentially invariant. At pH 5.8, the mutated peptides **TRI-H**K22Q and **TRI-EH** have very similar affinities and reduction potentials (Table 4), although they have higher Cu(I) affinities and lower Cu(II) affinities compared to the parent peptide **TRI-H**. It is worth noticing that **TRI-H** behaves quite differently compared to the mutated peptides at pH 5.8, possibility because of the lower pK_a's of the mutated peptides; however, it appears that Δ_{charge} of the residues at position 22 (one residue above the binding site, His23) does not have a dramatic influence on the affinities and redox properties of the peptide. On the basis of these observations, we chose to examine a series of peptide substitutions below the copper-binding site (positions 24 and 27) using the K22E-derived peptides, as this would allow for the widest range in Δ_{charge} (from 0 to −12).

As shown in Figure 5A, the Cu(I) affinities for the series of peptides containing a K22E substitution are related to the total charge around the copper binding site at both pH 5.8 and pH 7.4. As the total negative charge is increased, going from Δ_{charge} = 0 (**TRI-EH**E27K) to Δ_{charge} = −12 (**TRI-EH**K24E), the Cu(I) affinity decreased by about 2 orders of magnitude under both pH conditions. However, the Cu(II) affinities seemed to be relatively immune to the change in total charge. As shown in Figure 5B, at both pH 5.8 and pH 7.4, the change in Cu(II) affinities toward the peptides was minimal at a particular pH across the series of peptides with different total charges. It is interesting to note that unlike Cu(I), whose affinities remained essentially the same for a particular peptide at different pH with dissociation constants ranging from picomolar to femtomolar, Cu(II) was destabilized by at least 2 orders of magnitude when the pH decreased from 7.4 to 5.8, as shown in Figure 5B. The difference between Cu(I) and Cu(II) can be described more clearly when we compare the free energies of binding (section 4 in the Supporting Information) at a particular pH (Figure 6).

While reduction potentials for metalloproteins and small molecules are often determined by direct electrochemical methods, one may extract the same information by determining the protein binding affinities of the metals in both oxidation states and applying the Nernst equation. This approach has the added benefit that it allows one to track directly the behavior of interest (e.g., reaction rates) not only against the reduction potential but also to see whether correlations associated with a specific oxidation level exist. The reduction potentials of the Cu(II)/Cu(I)−peptide systems were calculated using the methodology shown in Scheme 1 and eq 2, where the value $E^{\circ}_{Cu,aq}$ = 0.159 V vs NHE was utilized (Table 4).[36,52] Since the free energy of binding for Cu(I) varies with amino acid substitution more than that of Cu(II) (Figure 6), the change in the calculated reduction potential is dominated by the variation of the Cu(I) affinity. This is true under both pH conditions; however, the change in potential between pH conditions is due to the stabilization of Cu(II) upon acidification. The linear regressions for the trends following amino acid substitutions resulted in two parallel lines, the distance between which was about 100 mV (Figure 7). This value corresponds to a 1 H$^+$ per

dx.doi.org/10.1021/ja406648n | J. Am. Chem. Soc. 2013, 135, 18096−18107

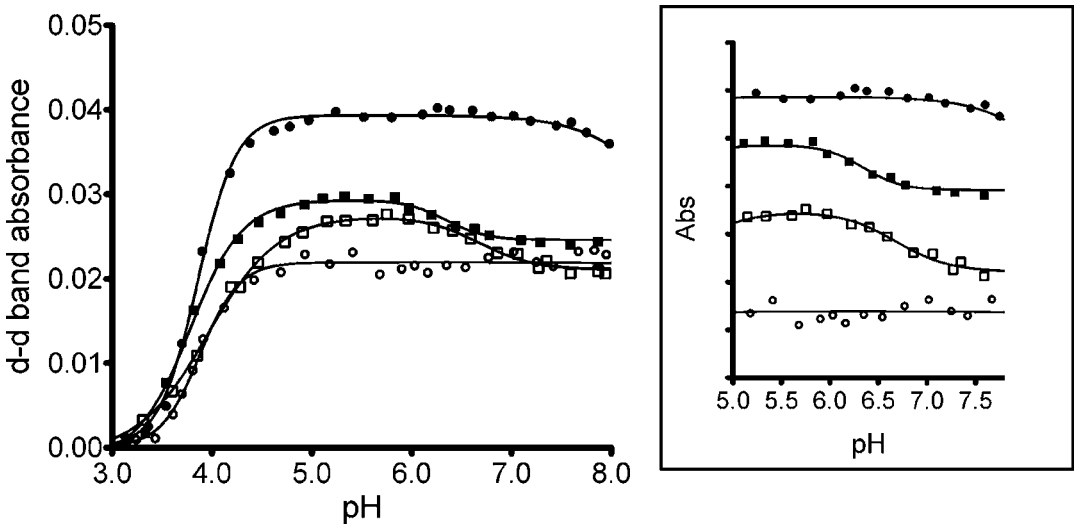

Figure 4. Changes in Cu(II) d−d band absorbance when Cu(II) was bound to (●) **TRI-H** ($\Delta_{charge} = 0$); (○) **TRI-EH**E27K ($\Delta_{charge} = 0$); (■) **TRI-EH** ($\Delta_{charge} = -6$); and (□) **TRI-EH**K24E ($\Delta_{charge} = -12$). The inset shows differences in the evolution of the Cu(II)−peptide d−d band, revealing different pK_a values (same symbols).

Table 3. Cu(I) and Cu(II) Dissociation Constants at pH 5.8 and pH 7.4

		K_d/M			
		Cu(I)		Cu(II)	
peptide	Δ_{Charge}	pH 5.8	pH 7.4	pH 5.8	pH 7.4
TRI-H[a]	−	3.09(66) × 10^{-12}	2.00(61) × 10^{-13}	4.04(83) × 10^{-8}	8.69(112) × 10^{-9}
TRI-HK22Q	−3	2.37(27) × 10^{-14}	4.12(114) × 10^{-14}	4.44(59) × 10^{-7}	3.80(106) × 10^{-9}
TRI-EHE27K	0	1.36(56) × 10^{-14}	2.07(27) × 10^{-15}	3.47(104) × 10^{-7}	1.45(71) × 10^{-9}
TRI-EHE27Q	−3	2.42(118) × 10^{-14}	1.76(41) × 10^{-14}	1.26(32) × 10^{-7}	3.76(72) × 10^{-9}
TRI-EH	−6	4.17(19) × 10^{-14}	1.12(43) × 10^{-13}	7.38(324) × 10^{-7}	6.39(258) × 10^{-9}
TRI-EHK24Q	−9	5.38(323) × 10^{-13}	8.06(509) × 10^{-14}	2.18(104) × 10^{-7}	3.73(203) × 10^{-9}
TRI-EHK24E	−12	3.52(9) × 10^{-13}	4.23(292) × 10^{-13}	4.92(225) × 10^{-7}	4.98(173) × 10^{-9}

[a]The data for **TRI-H** are from ref 36 and were collected at pH 5.9 and 7.4.

Table 4. Calculated Reduction Potentials Based on Cu(I) and Cu(II) Affinities

		$E°$(Cu−pep$_3$)/mV	
peptide	Δ_{Charge}	pH 5.8	pH 7.4
TRI-H[a]	−	402(8)	433(8)
TRI-HK22Q	−3	589(5)	450(10)
TRI-EHE27K	0	597(13)	504(13)
TRI-EHE27Q	−3	556(14)	474(8)
TRI-EH	−6	587(11)	440(14)
TRI-EHK24Q	−9	491(20)	435(21)
TRI-EHK24E	−12	522(12)	400(20)

[a]For **TRI-H**, calculations were based on the affinities at pH 5.9 and 7.4.

electron change in potential, which is consistent with the difference of 1.6 pH units for these measurements.

$$E^{\circ}_{Cu(pep)_3} = E^{\circ}_{Cu,aq} - \frac{2.303RT}{nF} \log \frac{K_{d,Cu(I)(pep)_3}}{K_{d,Cu(II)(pep)_3}} \quad (2)$$

XAS of Cu(I)(TRI-EH)$_3$. The XANES spectra of Cu(I)(**TRI-EH**)$_3$ and Cu(I)(**TRI-H**)$_3$ (Figure 8A) both show a modest-intensity peak at ∼8983 eV; this is typical of Cu(I) in an approximately trigonal environment.[53] The near identity of these spectra shows that there are only minor structural differences between the copper sites. The EXAFS data for Cu(I)(**TRI-EH**)$_3$ (Figure 8B,C) support this structural interpretation. The Fourier transform is dominated by a peak at $R \approx 1.5$ Å typical of Cu−N or Cu−O nearest-neighbor scattering, with pronounced outer-shell scattering typical of rigid ligands such as histidine. Quantitative fitting (Table 5) confirmed this structure. The nearest-neighbor distance of 1.93 Å is typical of three-coordinate Cu(I), and the outer-shell scattering can be modeled using three imidazole ligands; these results are quantitatively consistent with structural parameters reported previously for Cu(I)(**TRI-H**)$_3$.[36] Attempts to fit the data with a Cu−O shell in addition to or in place of one of the Cu−imidazole interactions did not give any improvement in the fit (Table S6 in the Supporting Information).

EPR Analyses of Cu(II)−Peptide Complexes. EPR spectra of Cu(II)(**TRI-H**)$_3$ were collected from pH 5.87 to pH 9.14, and they showed a transition of $A_{\|}$ and $g_{\|}$ from pH 7.80 to pH 9.14 (section 3 in the Supporting Information). The EPR parameters of Cu(II)(**TRI-EH**E27K)$_3$, Cu(II)(**TRI-EH**)$_3$, and Cu(II)(**TRI-EH**K24E)$_3$ at both pH 5.8 and 7.4 were in the same range as those of the parent peptide complex (Table 6). Specifically, $g_{\perp}$ is smaller than $g_{\|}$ and $A_{\|}$ is in the range of 17−19 mT for all of these complexes, indicative of a type 2 copper center with a high coordination number (4 or 5), which is consistent with the observed d−d bands in the UV−vis spectra.

dx.doi.org/10.1021/ja406648n | J. Am. Chem. Soc. 2013, 135, 18096−18107

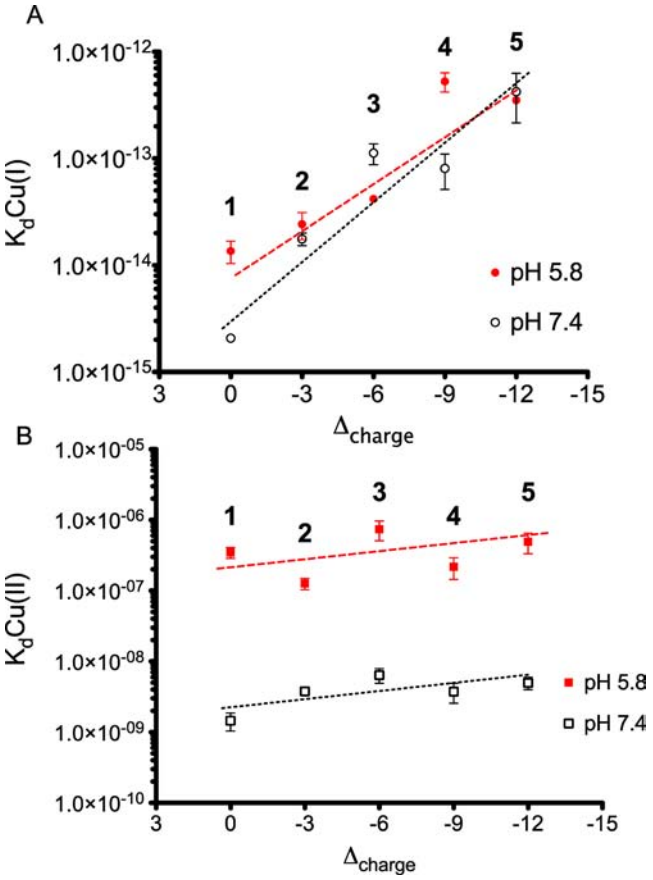

Figure 5. (A) Cu(I) dissociation constants and (B) Cu(II) dissociation constants with respect to Δ_{charge} at pH 5.8 and pH 7.4. Peptides: (1) **TRI-EH**E27K; (2) **TRI-EH**E27Q; (3) **TRI-EH**; (4) **TRI-EH**K24Q; (5) **TRI-EH**K24E. It should be noted that the *y* axes have log scales.

NiR Activity. The Cu–peptides exhibited NiR activity with different rates (Figure 9), all of which are pH-dependent. Specifically, as the total negative charge was increased from 0 to −12, the rates of the reaction increased about 4-fold. Moreover, the rates are also correlated to the calculated reduction potentials at pH 5.8 (Figure 10): as the calculated reduction potentials increase, the rates decrease. The turnover numbers (TONs) for these reactions, expressed as moles of electrons per mole of copper, were obtained. The TONs in 1 h are linearly associated with the local negative charge (Figure S6). As Δ_{charge} increased from 0 (**TRI-EH**E27K) to −12 (**TRI-EH**K24E), the TONs at pH 5.8 increased by one. For all of the NiR reactions, we did not observe any degradation of the enzyme 1.5 h after the reaction was initiated. Nitric oxide production was confirmed for the peptides showing the lowest and highest rates [Cu(**TRI-EH**E27K)$_3$ and Cu(**TRI-EH**K24E)$_3$, respectively] at pH 5.8 (section 8 in the Supporting Information).

DISCUSSION

The environment that surrounds redox sites plays a critical role in determining the redox potentials and pathways for electron flow in proteins. However, in most cases, multiple factors exert influence on the redox potential simultaneously, complicating the understanding of the structure–function relationship of a particular system. Conceptually, we can think of the energy associated with the redox process as the sum of the inner-sphere contributions, which directly point to the energy needed to add or remove an electron from the redox site, and outer-sphere contributions, which are related to the interaction of the redox site with the protein and solvent environment during the redox process.[54] In reality, more often than not a single change

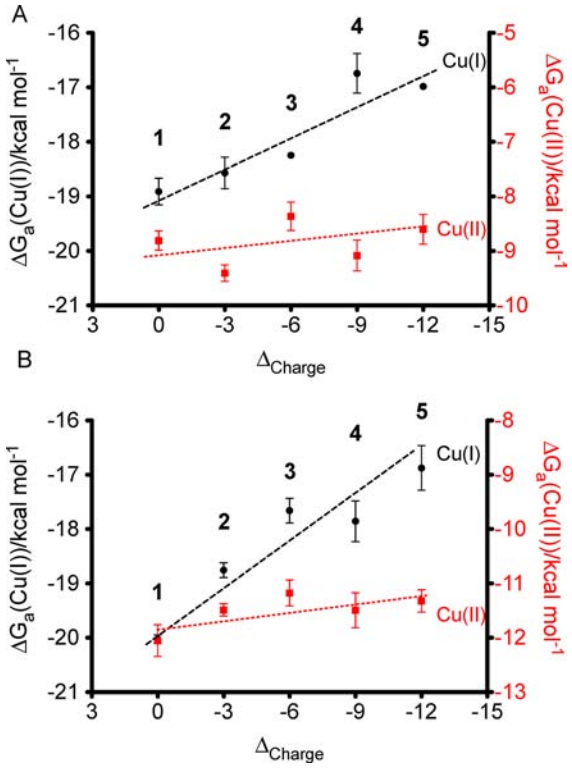

Figure 6. Free energies of binding for Cu(I) and Cu(II) at (A) pH 5.8 and (B) pH 7.4. Peptides: (1) **TRI-EH**E27K; (2) **TRI-EH**E27Q; (3) **TRI-EH**; (4) **TRI-EH**K24Q; (5) **TRI-EH**K24E.

Scheme 1

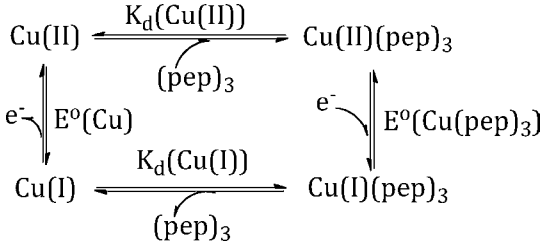

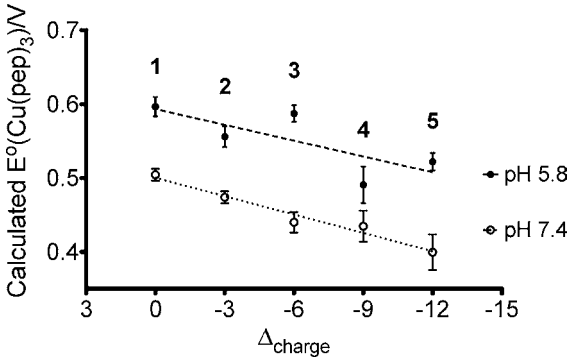

Figure 7. Calculated reduction potentials in relation to the changes of the local charge at pH 5.8 and pH 7.4. Peptides: (1) **TRI-EH**E27K; (2) **TRI-EH**E27Q; (3) **TRI-EH**; (4) **TRI-EH**K24Q; (5) **TRI-EH**K24E.

dx.doi.org/10.1021/ja406648n | J. Am. Chem. Soc. 2013, 135, 18096–18107

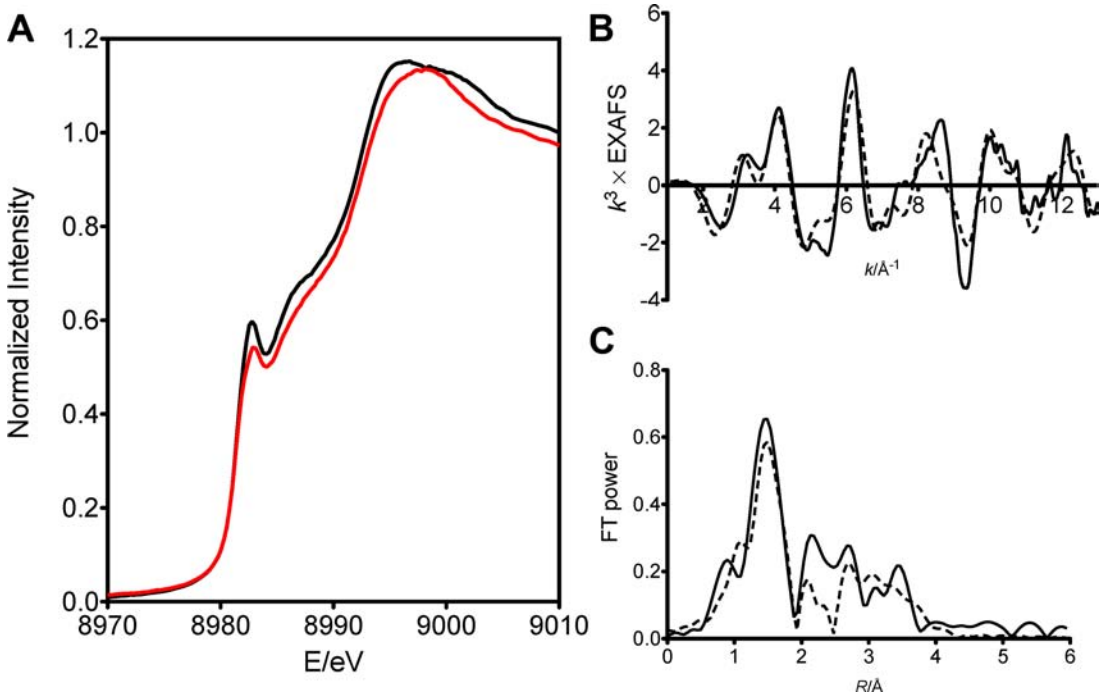

Figure 8. (A) XANES of Cu(I)(**TRI-H**)$_3$ at pH 7.4 (black line) and Cu(I)(**TRI-EH**)$_3$ at pH 8.5 (red line). (B) EXAFS of Cu(I)(**TRI-EH**)$_3$ at pH 8.5 (experimental data, solid line; fit, dashed line). (C) Fourier transform of the EXAFS data in *R* space (experimental data, solid line; fit, dashed line).

Table 5. EXAFS Fitting Parameters[a] for Cu(I)(TRI-EH)$_3$

first shell	R/Å	σ^2/Å^2	outer shells	R/Å	σ^2/Å^2
3 Cu(I)−N$^{(1)}$	1.93	0.008	3 Cu−C$^{(1)}$	2.91	0.012
			3 Cu−C$^{(2)}$	2.95	0.012
			3 Cu−N$^{(2)}$	4.05	0.010
			3 Cu−C$^{(3)}$	4.06	0.010

[a] $\Delta E_0 = -11.94$ eV, R (distance), and σ^2 (Debye−Waller factor) were the only freely variable parameters. The coordination number was held constant at 3, and the outer-shell parameters were calculated assuming a rigid imidazole ring. For a comparison of different models, see Table S6.

Table 6. EPR Parameters of Cu(II)(3SCC)$_3$ at pH 5.8 and pH 7.4

	pH 5.8				
peptide	$g_\perp$	$g_\parallel$	$A_\perp$/mT	$A_\parallel$/mT	A_{iso}/mT
Cu(II)(**TRI-H**)$_3$	2.05	2.28	0.64	18.58	6.62
Cu(II)(**TRI-EH**E27K)$_3$	2.06	2.27	0.68	17.36	6.24
Cu(II)(**TRI-EH**)$_3$	2.06	2.27	0.36	18.33	6.35
Cu(II)(**TRI-EH**K24E)$_3$	2.06	2.28	0.18	18.33	6.23
	pH 7.4				
peptide	$g_\perp$	$g_\parallel$	$A_\perp$/mT	$A_\parallel$/mT	A_{iso}/mT
Cu(II)(**TRI-H**)$_3$	2.05	2.27	0.64	18.58	6.62
Cu(II)(**TRI-EH**E27K)$_3$	2.05	2.27	1.07	17.50	6.55
Cu(II)(**TRI-EH**)$_3$	2.06	2.27	1.07	18.15	6.76
Cu(II)(**TRI-EH**K24E)$_3$	2.05	2.27	0.71	17.68	6.37

around the active site leads to a cascade of events that eventually modifies the redox properties, but it is challenging to track down the specific role of each event.

A significant amount of work has been done to understand the redox property modulations on systems containing heme cofactors or cupredoxin sites. It was reported as early as 1989

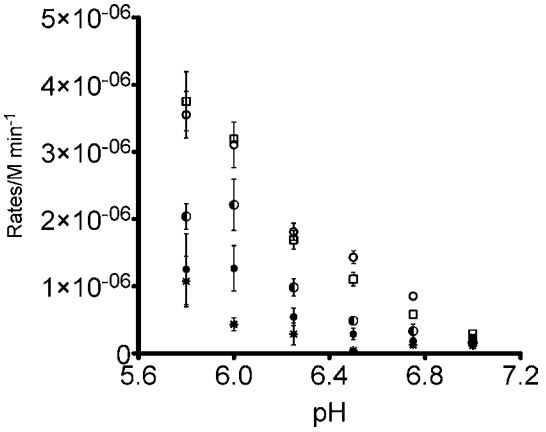

Figure 9. pH dependence of nitrite reduction rates. Peptides: (○) **TRI-EH**K24E ($\Delta_{charge} = -12$); (□) **TRI-EH**K24Q ($\Delta_{charge} = -9$); (◐) **TRI-EH** ($\Delta_{charge} = -6$); (●) **TRI-EH**E27Q ($\Delta_{charge} = -3$); (*) **TRI-EH**E27K ($\Delta_{charge} = 0$).

that mutating the valine (Val) residue into a charged or polar residue such as Glu, aspartate (Asp), or asparagine (Asn) leads to a decrease in the midpoint redox potential of recombinant myoglobin at 25 °C, which demonstrated that changing the electric field around the redox center would result in a substantial change in the redox thermodynamics of a particular system.[30] Specifically, the substitution of Val68 close to the distal site of the heme center with Glu or Asp led to a decrease of about 200 mV in the reduction potential, whereas Val68Asn resulted in an 80 mV decrease. Furthermore, the Dutton and Gibney groups showed that by varying the burial of heme in the hydrophobic core, heme peripheral substituents, heme-hydrophobic amino acids, and so on, they were able to modulate rationally the heme-protein redox potential over a range of a few hundred millivolts.[55−58] More recently, Lu and co-workers

dx.doi.org/10.1021/ja406648n | J. Am. Chem. Soc. 2013, 135, 18096−18107

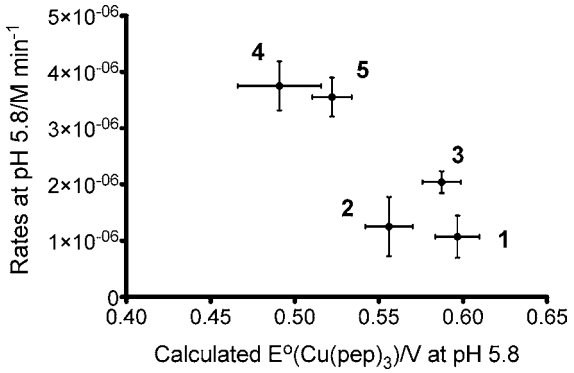

Figure 10. Rates at pH 5.8 in relation to the calculated reduction potentials at pH 5.8. Peptides: (1) **TRI-EH**E27K; (2) **TRI-EH**E27Q; (3) **TRI-EH**; (4) **TRI-EH**K24Q; (5) **TRI-EH**K24E.

demonstrated that the redox potential of a cupredoxin site in azurin can be tuned by modifying two important secondary coordination sphere interactions: hydrophobicity and H-bonding. Their work demonstrated an astounding shift in redox potentials, in some cases by as much as 700 mV, which extended even beyond the natural redox potential range of the protein.[59,60] To our current knowledge, there have been no systematic studies of the redox property modulations of the $Cu(His)_3$ site in a protein environment, despite its importance in the electron transfer or catalytic functions in native proteins.

Taking advantage of a de novo protein design approach, we took a known functional peptide, Cu(**TRI-H**)$_3$, and modified the local charge in a stepwise manner in order to observe changes in the reduction potentials and NiR activity of a series of peptides (Table 1). The rationale of the design was first to invert the charged residues Glu27 and Lys22, yielding **TRI-EH**E27K. Relative to the parent peptide **TRI-H**, the change in the overall charge (denoted as Δ_{charge}) for this peptide is 0. While this double mutation led to a significant shift in potential, we observed that there was no perturbation in the reduction potentials between copper complexes of **TRI-H** and **TRI-EH** at pH 7.4. We used the K22E mutation (**TRI-EH** scaffold) to evaluate a broader range of charge effects than would be available with **TRI-H**. We changed the residues of **TRI-EH** in a stepwise manner below the $Cu(His)_3$ site from positively charged residues to neutral and then negatively charged residues. Since three peptide strands self-assemble in aqueous solution above pH 5,[61] the resulting series of peptides have Δ_{charge} values of 0, −3, −6, −9, and −12. None of the residues involved in the mutations (Lys22, Lys24, and Glu27 in **TRI-H**) are inside the helix bundle, nor can they directly coordinate to the copper center (according to our PyMOL models shown in Figure 1). Hence, we did not expect to see first-coordination-sphere effects on the properties of the copper center. This de novo design strategy allowed us to vary the charge systematically in order to probe the subtle influence of surface charged residues on the stability constants of Cu(I) and Cu(II) protein forms and, subsequently, upon the redox properties and catalytic activities of these type 2 copper centers.

We first characterized the binding of the Cu(II) ion to the peptide as a function of pH using UV−vis spectroscopy, as shown in Figures 2−4. Before consideration of these spectra, it is worth recognizing that there are multiple pH-dependent reactions that can occur between pH 2.5 and 8.0 that can affect the chemistry in the system. First, the conversion of two-stranded coiled coils (2SCCs) to 3SCCs is known to occur upon the deprotonation of Glu at *e* positions with a pK_a of 4.0−4.5.[35,62] This behavior has been noted for several peptides of the **TRI** family, but most notably for **TRI-H**.[36] Second, the copper binding ligand can undergo deprotonation of the cationic imidazolium form, which does not bind copper, to the neutral imidazole, which binds to copper.[63] An ^{1}H NMR titration of (**TRI-H**)$_3$ showed that this deprotonation event occurs over the pH range 5.5−8.0 in the absence of metal.[36] Most likely, the presence of a Lewis acid shifts the imidazolium to imidazole equilibrium in favor of the neutral metal binding ligand, as has been reported for both Zn and Cu complexes with (**TRI-H**)$_3$.[36,42] Furthermore, under higher pH conditions the imidazole may be converted to the negatively charged imidazolate form, which also binds to copper efficiently. It is generally believed, however, that this equilibrium occurs at much higher pH values than investigated here. Additional carboxylic acid deprotonation events would be expected when Lys is substituted by Glu at position 22 and/or 24 for the mutated peptides. One would expect this deprotonation chemistry to occur in the general range of the pre-existing carboxylic acids at the *e* positions of the peptide. Under very high pH conditions (again above pH 8), deprotonation of the Lys side chain may become relevant, which could disrupt the 3SCCs; however, the conditions used in this study were unlikely to enter this basic range. Finally, when copper is bound, and if a water is bound to the copper, deprotonation of the Cu(II)-bound water could occur in the basic pH region.

An examination of the pH-dependent trends in Figure 4 demonstrates that **TRI-H**, **TRI-EH**E27K, **TRI-EH**, and **TRI-EH**K24E all exhibit a sharp rise in absorbance moving from pH 3 until the spectra level out by pH ∼5. Two major processes occur over this pH range. The first is the conversion of the 2SCCs to 3SCCs through deprotonation of Glu. This conversion for the apo-peptide is not reflected in these spectroscopic changes. The second process is the binding of Cu(II) to the 3SCCs, which is directly reflected by these spectra, as they arise from the d−d transition of Cu(II). Previous analysis of this copper site for Cu(II)(**TRI-H**)$_3$ using EPR spectroscopy suggested that this system is probably a five-coordinate Cu(II) with three coordinated imidazoles and two solvent molecules.[36] The UV−vis spectra of all these peptides are consistent with the same chromophore until at least pH 6.0. As the pH is raised to neutral conditions, peptides containing additional Glu (**TRI-EH**, and **TRI-EH**K24E) show an additional pH-dependent conversion ($pK_a^E \approx 6.5$). This process could be due to (A) deprotonation of the copper-coordinated water; (B) complexation of Glu22 to the copper; or (C) deprotonation of Glu22, leading to the formation of a hydrogen bond with either a coordinated His, a water H-bonded to a coordinated His or a bound water. We disfavor the explanations that Glu22 binds directly to Cu(II) or forms a hydrogen bond with coordinated water, as the orientation of the Glu on the helix places it too far from the metal center to interact in these ways. This observation leaves the most likely explanations for the pK_a^E in the 6−7 range for peptides containing the K22E mutations as deprotonation of metal-bound water or deprotonation of the glutamic acid leading to a H-bond formation between Glu22 and His23 (including a water bridging the two amino acids).

As shown in Figure 2B, Cu(II)(**TRI-H**)$_3$, which does not contain the K22E modification, exhibits a second significant absorption change at higher pH with a pK_a^W of 8.53. This is thought to be associated with the deprotonation of the Cu(II)-

dx.doi.org/10.1021/ja406648n | J. Am. Chem. Soc. 2013, 135, 18096−18107

bound water into a Cu(II)-bound hydroxide because the blue shift upon this deprotonation is in accordance with the prediction of the same process in an equatorially coordinated Cu(II) complex.[64] Spectral perturbations over this range were also observed in the EPR spectra of Cu(II)(**TRI-H**)$_3$. As the pH increased from 7.80 to 9.14, $g_{\|}$ decreased from 2.27 to 2.26 while $A_{\|}$ increased from 18.58 to 19.29 mT (Table S2). This observed trend is consistent with the reported case of copper-bound water deprotonation at the type 2 copper center in the mercury derivative of laccase.[65] This piece of evidence, combined with the transformation of the UV−vis spectra in this pH region, leads us to believe that the pK_a^w at 8.53 for Cu(II)(**TRI-H**)$_3$ corresponds to a Cu(II)-bound water deprotonation, producing a Cu(His)$_3$(OH)(OH$_2$)$_{0-1}$ species. Also consistent with the UV−vis spectra, the Cu(II)(**TRI-H**)$_3$ EPR spectra stay unchanged in the pH region 5.8 to 7.4, indicating that Cu(II) is likely to maintain a Cu(His)$_3$(OH$_2$)$_{1-2}$ coordination with three quasi-in-plane imidazoles and one or two water molecules.[36]

In contrast, for the **TRI-EH** series of peptides, we observed different EPR parameters at pH 5.8 and 7.4. For the "charge-flipped" peptide Cu(II)(**TRI-EH**E27K)$_3$, $g_{\|}$ stayed the same while $A_{\|}$ increased by 0.14 mT and the isotropic hyperfine splitting constant A_{iso} increased by 0.31 mT (Table 6). Similar changes in $g_{\|}$ and A_{iso} occurred for Cu(II)(**TRI-EH**)$_3$. For Cu(II)(**TRI-EH**K24E)$_3$, however, both $g_{\|}$ and $A_{\|}$ decreased significantly while $A_{\perp}$ increased, leading to an increased A_{iso}. In summary, the A_{iso} of the **TRI-EH** series of copper−peptide complexes increased when pH rose from 5.8 to 7.4, indicating a higher spin density at the copper center. The changes in the other EPR parameters are dissimilar to those of Cu(II)(**TRI-H**)$_3$ in a higher pH region (7.8 to 9.1), which implies that this equilibrium (corresponding to p$K_a^E \approx 6.5$) is probably not a Cu(II)-bound water deprotonation.

Considering the combined observations, we assign the pK_a^E at ∼6.5 for some of the **TRI-EH** peptides to a protonation equilibrium of a glutamate side chain (probably at position 22), which can become a hydrogen-bond acceptor for the imidazole proton at position 23 (or a water bridging the two amino acids). This H-bond leads to the variance of both the UV−vis and EPR spectral parameters of the Cu(II) center. Consistent with this assignment, when the same pH titration was carried out for Cu(II)(**TRI-H**K24E)$_3$, where the Glu was placed at position 24 instead of position 22, we did not observe a protonation equilibrium in this low pH range (Figure S4 and Table S1). For the "charge-flipped" peptide Cu(II)(**TRI-EH**E27K)$_3$, one might have expected it to behave more similarly to the other **TRI-EH** peptides having a lower pK_a^E; however, models suggest that Glu22 can interact with Lys27 in **TRI-EH**E27K, which would weaken the H-bonding interaction of Glu22 with His23. This putative H-bond would lead to a less acidic Cu(II), which would increase the pK_a^w for the Cu(II)-bound water deprotonation in these peptides. Correspondingly, we observed a higher pK_a^w (9.6−9.8) for the **TRI-EH** series of peptides, which we assign as the deprotonation of the Cu(II)-bound water (Table S1).

At pH 5.8 and pH 7.4, we determined the binding affinities of Cu(I) and Cu(II) to the series of peptides prepared in this work in order to evaluate the reduction potentials and the impact of protein mutations at both oxidation levels (Table 3 and Figures 5 and 6). These peptides were prepared in order to examine the effect of increased local negative charge on the stabilities of Cu(I) and Cu(II) within the hydrophobic core. It was thought that the Cu(II) state would be more greatly stabilized by higher negative charge, decreasing the reduction potential of the system. While the reduction potentials (Table 4) were made less positive by increasing the local negative charge, contrary to our expectation, this shift occurred as a result of Cu(I) destabilization rather than Cu(II) stabilization. These results are most clearly visualized by comparing the free energies of binding shown in Figure 6.

In contrast, Rorabacher and co-workers have reported a series of potentially tetradentate copper complexes that vary neutral nitrogen or sulfur donors over the range N_4 to NS_3. The reduction potentials of these compounds were strongly influenced by the stability constants of the Cu(II) oxidation level rather than those of the Cu(I) complexes.[66,67] In particular, an increase in the stability constants of the Cu(II) complexes by as much as 10^4−10^5-fold was observed upon substitution of thioether sulfurs for unsaturated nitrogens; at the same time, the stability constants of the Cu(I) complexes were maintained in the range 10^{14}−10^{16} M^{-1}. These changes led to differences in the reduction potentials that spanned 1.5 V.[66] The redox potentials were also observed to be pH-dependent below pH 5 (but invariant above this pH) because of the acid−base chemistry of the ligand.[68] Important differences between these models and our system include the choice of ligands (neutral thioethers and pyridyl groups), the lack of potential H-bond acceptors (such as glutamate), the lack of charge variation across the series, and the possibility of a tertiary amino nitrogen atom that could serve as a fourth ligand. Hence, our system provides a more biologically relevant example to assess how electrostatic and H-bonding influence copper protein reduction potentials.

As shown in Figure 5, the relative Cu(I) or Cu(II) affinity change across the series of designed protein mutants is independent of pH, as demonstrated by the invariant slopes of the lines for the two oxidation states. This statement is not intended to suggest that pH is not important in this system, as marked effects on both the Cu(II) stability and reduction potential are seen. As was shown, the Cu(I) stabilities are more sensitive to protein modification [$\Delta(\Delta G_a^{Cu(I)}) \approx 2$ kcal/mol vs $\Delta(\Delta G_a^{Cu(II)}) \approx 0.7$ kcal/mol], whereas one sees that the Cu(II) affinities are more sensitive to pH adjustment [$(\Delta G_a^{Cu(I)})_{pH\ 7.4} - (\Delta G_a^{Cu(I)})_{pH\ 5.8} \approx 0.5$ kcal/mol vs $(\Delta G_a^{Cu(II)})_{pH\ 7.4} - (\Delta G_a^{Cu(II)})_{pH\ 5.8} \approx 3.5$ kcal/mol]. Thus, the trend is that as the negative charge around the copper center is increased via protein modification, Cu(I) is destabilized and the reduction potential becomes less positive. In contrast, as the pH is lowered, the Cu(II) affinity decreases and the reduction potential becomes more positive (Table 4). Within the series there is shift in potential of ∼100 mV in going from pH 7.4 to pH 5.8 for any peptide, providing a slope of ∼60 mV/pH unit, which indicates that the change in potential is dependent upon a single proton per electron. The differences between the copper affinities lead to the two parallel lines shown in Figure 7. Thus, by controlling the peptide sequence and the pH, one can systematically vary the reduction potential in this system by nearly 200 mV.

The observed trends can be explained by the change in H-bonding and salt-bridging interactions around the copper center upon protein mutations under different pH conditions. The mutation of Lys at position 22 into a Glu would likely lead to an H-bonding interaction between the carboxylic acid/carboxylate from Glu and the imidazole from His (or a water bridging the two amino acids), and therefore, we see pH-

dependent Cu(II) affinities and reduction potentials. Variations of the other charged residues would alter the salt-bridging interactions, leading to differences in the electron-donating abilities of the imidazoles or structural changes to the Cu(I) center. Consistent with this idea, we see that **TRI-H** exhibits a modest shift to a *less* positive potential ($\Delta = -30$ mV) in going from pH 7.4 to pH 5.9 while all of the peptides with Gln or Glu at position 22 show significant shifts to *more* positive potentials ($\Delta = +60$ to $+140$ mV) as the pH is decreased (Table 4). One possible H-bonding system that supports both the pH trends in Cu(II) binding and the impact of side-chain mutations of the Cu(I) affinities is provided in section 9 in the Supporting Information.

Alteration of the peptide in the layer above the copper site (position 22) has virtually no effect on the reduction potential of the system (at pH 7.4: **TRI-H**, E° = 433 mV; **TRI-H**K22Q, E° = 450 mV; **TRI-EH**, E° = 440 mV). In general, with peptides containing the K22E modification (i.e., those where mutations are made to **TRI-EH**), one observes that increasing the side-chain positive charge below the metal site causes significant stabilization of the Cu(I) oxidation level, while the Cu(II) state is mildly stabilized by the same mutation. Thus, if we take **TRI-EH** as the parent peptide, replacing Lys at position 24 with Gln and Glu progressively destabilizes Cu(I) binding, whereas converting Glu27 into Gln or Lys yields much higher Cu(I) affinities. If this were solely an electrostatic effect, one might expect the opposite trend for the Cu(I) affinity (as more positive charge around the positive metal should destabilize binding) and that a greater effect would be observed for the Cu(II) level (as charge repulsion would be greater). These observations suggest that an alternative explanation is required. Our best explanation is that this may again reflect H-bonding and salt bridging between the different surface residues. In the case of Cu(I)−peptide complexes, the dominant factor may be structural perturbations that occur at the metal center.

In order to form an effective geometry for directional H-bonding and salt-bridging interactions, the imidazoles may need to reorient to minimize the conformational changes on the peptide backbone, leading to a more trigonal-planar or tetrahedral Cu(I) structure. Our present best explanation for the decreased Cu(I) affinity as the H-bond is formed is based on this geometric argument rather than electronic factors. It was previously shown that Cu(I) in **TRI-H** forms a distorted trigonal-planar structure.[36] We examined the parent peptide for the series of peptides reported here: **TRI-EH**, forming a direct comparison to **TRI-H**. XANES data revealed that the Cu(I) coordination number did not change when we substituted a Glu for the Lys at position 22, which is consistent with the fact that the affinity of Cu(I) in this pH range does not change much in going from **TRI-H** to **TRI-EH**. The subtle differences of the edge structure are consistent with small changes in the symmetry of the site. For example, the small decrease in the intensity of the peak at 8983.4 eV would be consistent with a change from a more T-shaped geometry to a more trigonal-planar structure,[53] consistent with our predictions. The EXAFS fits suggest relatively large disorder in the Cu(I) site. The fitted σ^2 values for Cu(I)(**TRI-EH**)$_3$ are smaller than those found for Cu(I)(**TRI-H**)$_3$,[36] indicating that there is somewhat less variation in the Cu−N distances for Cu(I)(**TRI-EH**)$_3$. This is consistent with the suggestion, based on the XANES, that the Cu(I) site in Cu(I)(**TRI-EH**)$_3$ is somewhat more symmetric than that in Cu(I)(**TRI-H**)$_3$.

It is likely that a similar, possibly even more rigid trigonal plane exists for **TRI-EH**E27K because of the formation of an interhelical H-bonding network connecting His23, Glu22, and Lys27 from the adjacent strands, which would hold the copper-coordinating His ligand in a relatively constrained environment (Figure S9). This is of great relevance to the rack-induced binding hypothesis proposed for blue copper electron transfer centers in native proteins.[69] This hypothesis suggests that the protein matrix is responsible for maintaining a proper metal coordination environment and fine-tuning the redox potential to facilitate electron transfer processes. Of great interest to us is a report that demonstrates the importance of a hydrogen bond close to the type 1 copper center in plastocyanin, which contributes to the rigidity of the coordinating environment of the type 1 copper center.[70] The higher reduction potential of Cu(**TRI-EH**E27K)$_3$ is reflective of the rigidity at the copper centers that favors a trigonal Cu(I). This can explain the difference between our system and Rorabacher's complexes mentioned earlier. In our case, the Cu(II) state is more structurally dynamic while Cu(I) is more rigid. As a result, the modulation of reduction potentials is dominated by the variance in the Cu(I) state. In Rorabacher's case, the small-molecule scaffold has a similar level of rigidity for both oxidation states, so the stability constants of the higher oxidation state are more dramatically influenced by the number and nature of the donor atoms, the chelate ring size, and the general ligand topology, while little variation is observed for the lower oxidation states.

For **TRI-EH**K24E, while Glu22 forms a hydrogen bond with His23 (or a water bridging the two amino acids), the charge repulsion between Glu22, Glu24, and Glu27 on the neighboring helices might force the imidazoles to adopt a tetrahedral geometry. Such perturbations in geometry are not required for the Cu(II) site, as it is believed that this ion is already five-coordinate with the imidazoles no longer planar. For Cu(II), the influence of salt-bridging and H-bonding effects are not as pronounced under a specific pH condition. This point may be understood most simply as follows: Cu(II) is much more Lewis acidic, which should lead to acidification of the coordinated imidazole proton. Thus, regardless of competing salt bridges, the Glu22 substitution may lead to a hydrogen bond of sufficient stability not to be diminished significantly by salt-bridging effects and protein mutations.

We next examined how side-chain modifications would affect the known catalytic activities of this system. The nitrite reductase (NiR) activity of these peptides is expressed in terms of the rate of ascorbate consumption. The influence of the reduction potential on the NiR rate is clearly revealed by an examination of the rates at a constant pH. At pH 5.8, for the **TRI-EH** series of peptides, the higher the reduction potential, the lower the rate (Figure 10). The reduction potential changes from 597 mV (**TRI-EH**E27K) to 491 mV (**TRI-EH**K24Q), leading to a 3.5-fold increase in rate [from $1.07(65) \times 10^{-6}$ to $3.75(76) \times 10^{-6}$ M min^{-1}]. While there is an impressive linear correlation between the rates and the reduction potentials, one must use caution to ascribe this effect to electron transfer since our studies show that the rapid reduction of Cu(II) to Cu(I) by ascorbate cannot be rate-limiting. More likely, the significant reorganization energy due to the change in coordination geometry from Cu(I) [three-coordinate] to Cu(II) [five-coordinate] limits the observed rates.

The nitrite reduction rates also increased markedly with decreasing pH, which was observed for both the parent

dx.doi.org/10.1021/ja406648n | J. Am. Chem. Soc. 2013, 135, 18096−18107

peptide[36] and the mutated peptides (Table S4). The native CuNiR is also reported to exhibit pH-dependent activities that are proposed to be closely related to both the electron transfer process and the nitrite binding step at the catalytic site.[23] In our case, since we do not have a type 1 electron transfer site and the reduction of the Cu(II) by ascorbate is much faster than the catalytic reaction, the observed pH dependence is likely correlated to steps during the nitrite reduction catalytic cycle. Since the full chemical reaction requires 2 equiv of protons, it is not surprising to see that the reaction rates are higher at a lower pH. Quantitatively, when the pH decreases from 7.0 to 5.8, the proton concentration in the solution $[H^+]$ increases about 16-fold; if the rate of the reaction were directly proportional to $[H^+]^2$, it should have increased by 256-fold. Instead, an increase in rate of ∼10-fold was observed for **TRI-H**. The rates for the **TRI-EH** series of peptides similarly increased by 10−16-fold when the pH changed from 7.0 to 5.8 (Table S4). If one fits a plot of log(initial rate) versus pH for **TRI-H** to the expression log(initial rate) = $a - b$·pH, the b coefficient, which corresponds to the proton order of the reaction, is 0.85. Thus, while the stoichiometric reaction requires two protons, the rate-limiting step is dependent on a single proton. The second proton is necessary once the hydroxide leaving group is formed.[24,71,72]

For all of the **TRI-EH** peptides, when the pH decreased from 7.4 to 5.8, the reduction potential increased by about 100 mV. If this were the only factor influencing the reaction rate, the NiR rate should have decreased. It is worth noticing that the rates are very low at pH 7.0, so the NiR rates were analyzed only at pH 5.8. As a result, for a specific peptide, when the pH decreases from 7.0 to 5.8, the participation of a proton in the rate-limiting step directly enhances the rate, while the significant structural change upon conversion from Cu(I) to Cu(II) (reflected as an increased reduction potential) impedes the reaction. This is consistent with the trends observed when comparing the peptides at a fixed proton concentration. Combining these two opposite effects, we observed a 10−16-fold rate increase when the pH decreased from 7.0 to 5.8.

It should be noted that the NiR rate versus reduction potential correlation at a constant pH should be interpreted with caution, as it compares only peptides that contain a Glu at position 22. If one compares the parent peptide **TRI-H** and the "charge-flipped" peptide **TRI-EH**E27K at pH 5.8, the situation is different. The reduction potential of **TRI-EH**E27K is about 200 mV more positive than that of **TRI-H**, but its NiR rate is only 2 times less than that of the parent peptide. Using the correlation in Figure 9, one would have expected a 6-fold differential between these two peptides if reduction potential *alone* were the determining factor. In general, despite the fact that the **TRI-EH** peptides have much more positive reduction potentials, they have, as a group, greater than (or approximately equal) activities compared with **TRI-H**. For example, comparing the rates of Cu(**TRI-H**)$_3$ and Cu(**TRI-EH**)$_3$ at pH 5.8 (Table S4) shows two peptides with similar activities but strongly divergent reduction potentials. This observation points to the importance of the Glu at position 22 for enhancing the rates and suggests that the other substitutions made in this series moderate the beneficial impact of this Glu22 on catalysis.

CONCLUSION

We have reported here a systematic approach of modulating the reduction potentials and NiR activities within a self-assembled peptidic framework by stepwise modifications that influence the local charge. These modifications vary the deprotonation equilibria of the Cu(II)−peptide complexes, which have a direct impact on the Cu(II) affinities to the apo-peptide under different pH conditions. At a specific pH, the influence of the mutations is reflected by the linear correlation of the Cu(I)−peptide affinity and Δ_{charge}. Reduction potentials were calculated from the Cu(I) and Cu(II) affinities to the apo-peptides. For a particular peptide, the difference in the reduction potentials under different pH conditions originates from the change in Cu(II) affinity; at a specific pH, the difference in the reduction potentials for the **TRI-EH** series of peptides is dominated by the variance in the Cu(I) affinities, which could be the result of the structural perturbation of Cu(I) coordination upon the alteration of charged residues. Moreover, all of these metalloenzymes exhibit pH-dependent NiR activities. For a specific peptide, the NiR rates are governed by the proton concentration and the reduction potentials under different pH conditions. At a specific pH, the reduction potentials correlate with the observed rates, but other factors, such as the formation of the substrate−enzyme complex, formation of the product−enzyme complex, and product release, may also play a role in determining the NiR rates. In particular, the data implicate a key role for a Glu at position 22 in enhancing catalysis. This is likely due to either a hydrogen bond to His23 (or a water bridging the two amino acids) or an interaction with the copper-bound substrate.

This study demonstrates that even in highly simplified scaffolds, attempts to change the local charge around the active site may cause multiple interactions that can vary the redox properties and activities in distinct ways. Nevertheless, this de novo design approach allows us to begin to peel the onion layer by layer. Although we still have not drawn a complete picture of the chemistry in this series of peptides, we have demonstrated our ability to isolate different factors (pH, affinities, reduction potentials, etc.) and to compare and analyze the effects in a multidimensional way. In conclusion, this work showcases the strength of de novo protein design to anchor the in-depth understanding of fundamental interactions that modulate the redox properties and NiR activities for a type 2 copper center, which provides interesting insights into future work on model chemistry in general.

ASSOCIATED CONTENT

Supporting Information

Detailed data fitting process, calculations, additional characterizations, and PyMOL models. This material is available free of charge via the Internet at http://pubs.acs.org.

AUTHOR INFORMATION

Corresponding Author

vlpec@umich.edu

Notes

The authors declare no competing financial interest.

ACKNOWLEDGMENTS

V.L.P. thanks the National Institutes of Health for financial support of this research (ES012236). F.Y. thanks the Department of Chemistry of the University of Michigan for a research fellowship. Portions of this research were carried out at the Stanford Synchrotron Radiation Lightsource, a Directorate of SLAC National Accelerator Laboratory and an Office of

Science User Facility operated for the U.S. Department of Energy Office of Science by Stanford University.

REFERENCES

(1) Prabhulkar, S.; Tian, H.; Wang, X.; Zhu, J.-J.; Li, C.-Z. *Antioxid. Redox Signaling* **2012**, *17*, 1796−1822.
(2) Fedurco, M. *Coord. Chem. Rev.* **2000**, *209*, 263−331.
(3) Groves, J. T. *Proc. Natl. Acad. Sci. U.S.A.* **2003**, *100*, 3569−3574.
(4) Umena, Y.; Kawakami, K.; Shen, J.-R.; Kamiya, N. *Nature* **2011**, *473*, 55−60.
(5) Castiglione, N.; Rinaldo, S.; Giardina, G.; Stelitano, V.; Cutruzzolà, F. *Antioxid. Redox Signaling* **2012**, *17*, 684−716.
(6) Klinman, J. P. *Chem. Rev.* **1996**, *96*, 2541−2562.
(7) Averill, B. A. *Chem. Rev.* **1996**, *96*, 2951−2964.
(8) Crichton, R. R.; Pierre, J. L. *Biometals* **2001**, *14*, 99−112.
(9) Solomon, E. I.; Szilagyi, R. K.; DeBeer George, S.; Basumallick, L. *Chem. Rev.* **2004**, *104*, 419−458.
(10) Rosenzweig, A. C.; Sazinsky, M. H. *Curr. Opin. Struct. Biol.* **2006**, *16*, 729−735.
(11) MacPherson, I. S.; Murphy, M. E. P. *Cell. Mol. Life Sci.* **2007**, *64*, 2887−2899.
(12) Solomon, E. I.; Sundaram, U. M.; Machonkin, T. E. *Chem. Rev.* **1996**, *96*, 2563−2606.
(13) Solomon, E. I.; Ginsbach, J. W.; Heppner, D. E.; Kieber-Emmons, M. T.; Kjaergaard, C. H.; Smeets, P. J.; Tian, L.; Woertink, J. S. *Faraday Discuss.* **2011**, *148*, 11−39.
(14) Solomon, E. I.; Hadt, R. G. *Coord. Chem. Rev.* **2011**, *255*, 774−789.
(15) Solomon, E. I.; Chen, P.; Metz, M.; Lee, S.-K.; Palmer, A. E. *Angew. Chem., Int. Ed.* **2001**, *40*, 4570−4590.
(16) Hannan, J. P.; Busch, J. L. H.; Breton, J.; James, R.; Thomson, A. J.; Moore, G. R.; Davy, S. L. *J. Biol. Inorg. Chem.* **2000**, *5*, 432−447.
(17) Chufán, E. E.; Prigge, S. T.; Siebert, X.; Eipper, B. A.; Mains, R. E.; Amzel, L. M. *J. Am. Chem. Soc.* **2010**, *132*, 15565−15572.
(18) Evans, J. P.; Blackburn, N. J.; Klinman, J. P. *Biochemistry* **2006**, *45*, 15419−15429.
(19) Kline, C. D.; Mayfield, M.; Blackburn, N. J. *Biochemistry* **2013**, *52*, 2586−2596.
(20) Prigge, S. T.; Eipper, B. A.; Mains, R. E.; Amzel, L. M. *Science* **2004**, *304*, 864−867.
(21) Libby, E.; Averill, B. A. *Biochem. Biophys. Res. Commun.* **1992**, *187*, 1529−1535.
(22) Moura, I.; Moura, J. J. *Curr. Opin. Chem. Biol.* **2001**, *5*, 168−175.
(23) Pinho, D.; Besson, S.; Brondino, C. D.; de Castro, B.; Moura, I. *Eur. J. Biochem.* **2004**, *271*, 2361−2369.
(24) Tocheva, E. I.; Rosell, F. I.; Mauk, A. G.; Murphy, M. E. P. *Science* **2004**, *304*, 867−870.
(25) Jacobson, F.; Pistorius, A.; Farkas, D.; De Grip, W.; Hansson, O.; Sjölin, L.; Neutze, R. *J. Biol. Chem.* **2007**, *282*, 6347−6355.
(26) Gray, H. B.; Malmström, B. G.; Williams, R. J. P. *J. Biol. Inorg. Chem.* **2000**, *5*, 551−559.
(27) Saab-Rincón, G.; Valderrama, B. *Antioxid. Redox Signaling* **2009**, *11*, 167−192.
(28) Matsuda, T.; Warshel, A. *Biochemistry* **1986**, *25*, 1675−1681.
(29) Kuila, D.; Fee, J. A. *J. Biol. Chem.* **1986**, *261*, 2768−2771.
(30) Varadarajan, R.; Zewert, T. E.; Gray, H. B.; Boxer, S. G. *Science* **1989**, *243*, 69−72.
(31) Hellwig, P.; Behr, J.; Ostermeier, C.; Richter, O. M.; Pfitzner, U.; Odenwald, A.; Ludwig, B.; Michel, H.; Mäntele, W. *Biochemistry* **1998**, *37*, 7390−7399.
(32) Baltzer, L.; Nilsson, H.; Nilsson, J. *Chem. Rev.* **2001**, *101*, 3153−3163.
(33) DeGrado, W. F.; Summa, C. M.; Pavone, V.; Nastri, F.; Lombardi, A. *Annu. Rev. Biochem.* **1999**, *68*, 779−819.
(34) Bryson, J. W.; Betz, S. F.; Lu, H. S.; Suich, D. J.; Zhou, H. X.; O'Neil, K. T.; DeGrado, W. F. *Science* **1995**, *270*, 935−941.
(35) Ghosh, D.; Pecoraro, V. L. *Inorg. Chem.* **2004**, *43*, 7902−7915.
(36) Tegoni, M.; Yu, F.; Bersellini, M.; Penner-Hahn, J. E.; Pecoraro, V. L. *Proc. Natl. Acad. Sci. U.S.A.* **2012**, *109*, 21234−21239.
(37) Ghadiri, M. R.; Case, M. A. *Angew. Chem., Int. Ed. Engl.* **1993**, *32*, 1594−1597.
(38) Tanaka, T.; Mizuno, T.; Fukui, S.; Hiroaki, H.; Oku, J.-I.; Kanaori, K.; Tajima, K.; Shirakawa, M. *J. Am. Chem. Soc.* **2004**, *126*, 14023−14028.
(39) Kiyokawa, T.; Kanaori, K.; Tajima, K.; Koike, M.; Mizuno, T.; Oku, J. J.-I. I.; Tanaka, T. *J. Pept. Res.* **2004**, *63*, 347−353.
(40) Hong, J.; Kharenko, O. A.; Ogawa, M. Y. *Inorg. Chem.* **2006**, *45*, 9974−9984.
(41) Hong, J.; Kharenko, O. A.; Fan, J.; Xie, F.; Petros, A. K.; Gibney, B. R.; Ogawa, M. Y. *Angew. Chem., Int. Ed.* **2006**, *45*, 6137−6140.
(42) Zastrow, M. L.; Peacock, A. F. A.; Stuckey, J. A.; Pecoraro, V. L. *Nat. Chem.* **2012**, *4*, 118−123.
(43) *Fmoc Solid Phase Peptide Synthesis: A Practical Approach*; Chan, W. C.; White, P. D., Eds.; The Practical Approach Series, Vol. *222*; Oxford University Press: New York, 2000.
(44) Farrer, B. T.; Harris, N. P.; Valchus, K. E.; Pecoraro, V. L. *Biochemistry* **2001**, *40*, 14696−14705.
(45) *The Protein Protocols Handbook*, 2nd ed.; Walker, J. M., Ed.; Humana Press: Totowa, NJ, 2002.
(46) Xiao, Z.; Loughlin, F.; George, G. N.; Howlett, G. J.; Wedd, A. G. *J. Am. Chem. Soc.* **2004**, *126*, 3081−3090.
(47) Xiao, Z.; Wedd, A. G. *Nat. Prod. Rep.* **2010**, *27*, 768−789.
(48) Xiao, Z.; Brose, J.; Schimo, S.; Ackland, S. M.; La Fontaine, S.; Wedd, A. G. *J. Biol. Chem.* **2011**, *286*, 11047−11055.
(49) George, G. N. *EXAFSPAK*; Stanford University: Stanford, CA, 2000; available at http://www-ssrl.slac.stanford.edu/exafspak.html.
(50) Ankudinov, A.; Rehr, J. *Phys. Rev. B* **1997**, *56*, R1712−R1716.
(51) Dimakis, N.; Bunker, G. *Phys. Rev. B* **2002**, *65*, No. 201103.
(52) Atkins, P.; Overton, T.; Rourke, J.; Weller, M.; Armstrong, F.; Hagerman, M. *Inorganic Chemistry*, 5th ed.; Freeman: New York, 2010.
(53) Kau, L. S.; Spira-Solomon, D. J.; Penner-Hahn, J. E.; Hodgson, K. O.; Solomon, E. I. *J. Am. Chem. Soc.* **1987**, *109*, 6433−6442.
(54) Perrin, B. S.; Ichiye, T. *J. Biol. Inorg. Chem.* **2013**, *18*, 103−110.
(55) Gibney, B. R.; Rabanal, F.; Reddy, K. S.; Dutton, P. L. *Biochemistry* **1998**, *37*, 4635−4643.
(56) Shifman, J. M.; Gibney, B. R.; Sharp, R. E.; Dutton, P. L. *Biochemistry* **2000**, *39*, 14813−14821.
(57) Gibney, B. R.; Isogai, Y.; Rabanal, F.; Reddy, K. S.; Grosset, A. M.; Moser, C. C.; Dutton, P. L. *Biochemistry* **2000**, *39*, 11041−11049.
(58) Gibney, B. R.; Dutton, P. L. *Adv. Inorg. Chem.* **2001**, *68*, 409−456.
(59) Marshall, N. M.; Garner, D. K.; Wilson, T. D.; Gao, Y.-G.; Robinson, H.; Nilges, M. J.; Lu, Y. *Nature* **2009**, *462*, 113−116.
(60) New, S. Y.; Marshall, N. M.; Hor, T. S. A.; Xue, F.; Lu, Y. *Chem. Commun.* **2012**, *48*, 4217−4219.
(61) Peacock, A. F. A.; Iranzo, O.; Pecoraro, V. L. *Dalton Trans.* **2009**, 2271−2280.
(62) Dieckmann, G. R.; McRorie, D. K.; Lear, J. D.; Sharp, K. A.; DeGrado, W. F.; Pecoraro, V. L. *J. Mol. Biol.* **1998**, *280*, 897−912.
(63) Sundberg, R. J.; Martin, R. B. *Chem. Rev.* **1974**, *74*, 471−517.
(64) Prenesti, E.; Daniele, P. G.; Prencipe, M.; Ostacoli, G. *Polyhedron* **1999**, *18*, 3233−3241.
(65) Tamilarasan, R.; Mcmillin, D. R. *Biochem. J.* **1989**, *263*, 425−429.
(66) Ambundo, E. A.; Deydier, M.; Grall, A. J.; Aguera-vega, N.; Dressel, L. T.; Cooper, T. H.; Heeg, M. J.; Ochrymowycz, L. A.; Rorabacher, D. B. *Inorg. Chem.* **1999**, *38*, 4233−4242.
(67) Rorabacher, D. B. *Chem. Rev.* **2004**, *104*, 651−697.
(68) Bernardo, M. M.; Heeg, J.; Schroeder, I. R. R.; Ochrymowycz, L. A.; Rorabacher, D. B. *Inorg. Chem.* **1992**, *31*, 191−198.
(69) Gray, H. B.; Malmström, B. G. *Comments Inorg. Chem.* **1983**, *2*, 203−209.
(70) Dong, S.; Ybe, J. A.; Hecht, M. H.; Spiro, T. G. *Biochemistry* **1999**, *38*, 3379−3385.
(71) Antonyuk, S. V.; Strange, R. W.; Sawers, G.; Eady, R. R.; Hasnain, S. S. *Proc. Natl. Acad. Sci. U.S.A.* **2005**, *102*, 12041−12046.
(72) Tavares, P.; Pereira, A. S.; Moura, J. J. G.; Moura, I. *J. Inorg. Biochem.* **2006**, *100*, 2087−2100.